Characterizing moisture exchange between the Hawaiian convective boundary layer and free troposphere using stable isotopes in water

Adriana Bailey,[1] Darin Toohey,[2] and David Noone[1]

Received 6 April 2013; revised 12 June 2013; accepted 9 July 2013; published 2 August 2013.

[1] The subtropical convective boundary layer (CBL) plays a critical role in climate by regulating the vertical exchange of moisture, energy, trace gases, and pollutants between the ocean surface and free troposphere. Yet bulk features of this exchange are poorly constrained in climate models. To improve our understanding of moisture transport between the boundary layer and free troposphere, paired measurements of water vapor mixing ratio and the stable isotope ratio $^{18}O/^{16}O$ are used to evaluate moist convective mixing and entrainment processes near the Big Island of Hawaii. Profile data from the island's east side are consistent with moist adiabatic processes below the trade wind temperature inversion. In contrast, profiles on the west side follow moist adiabatic lapse rates within discrete stable layers, suggesting moist convection sets the humidity structure of even the unsaturated regions around the island. Above the trade wind inversion, the transition from well-mixed boundary layer to free troposphere is characterized by a simple mixing line analysis, so long as the thermodynamic properties of the air mass at CBL top are known. Deviations from the mixing line identify thermodynamic boundaries in the atmospheric profile, which can persist from one day to the next. These findings indicate residual layers form during strong mixing events and regulate vertical moisture transport for multiple days at a time. Basic assumptions that synoptic-scale transport controls isotope ratios at CBL top are therefore not sufficient for describing moisture exchange between the boundary layer and free troposphere in the subtropics.

Citation: Bailey, A., D. Toohey, and D. Noone (2013), Characterizing moisture exchange between the Hawaiian convective boundary layer and free troposphere using stable isotopes in water, *J. Geophys. Res. Atmos.*, *118*, 8208–8221, doi:10.1002/jgrd.50639.

1. Introduction

[2] The trade wind temperature inversion in the subtropics separates air masses representing two hydrological extremes: the moist marine boundary layer below and the dry free troposphere above. Shallow convection transports boundary layer moisture across the inversion, while boundary layer growth simultaneously entrains warm and dry free tropospheric air. Since these mechanisms regulate the vertical transport of energy, moisture, trace gases, and pollutants, they play a significant role in climate. Yet while numerous laboratory [*Deardorff et al.*, 1980], observational [*Nelson et al.*, 1989; *Lenschow et al.*, 1999; *Bretherton et al.*, 1995; *Faloona et al.*, 2005; *Träumner et al.*, 2011], and modeling [*Sullivan et al.*, 1998; *Brooks and Fowler*, 2012] studies have investigated shallow convection and entrainment and their role in transporting material vertically, simulated climates remain sensitive to the choice of model parameterization [*Ayotte et al.*, 1996; *Stevens*, 2002; *Hu et al.*, 2010]. Such sensitivities suggest bulk features of vertical moisture exchange are still not fully understood. To improve our understanding of moisture transport processes in the subtropics, this paper uses conserved variables to evaluate bulk mixing properties associated with the entrainment region near the top of the convective boundary layer (CBL). Our findings suggest the transition from boundary layer to free troposphere is well characterized as a simple mixing problem so long as the thermodynamic properties of the air mass at CBL top are known.

[3] Conserved variable analyses provide a means to describe complex exchange processes in terms of a simple mixing problem. *Betts and Albrecht* [1987] introduced a mixing line analysis to characterize shallow convective detrainment and entrainment in the CBL using a conserved variable diagram of total water mixing ratio (q_T) and equivalent potential temperature (θ_E). In their approach, warm and moist tropical air from the well-mixed region of the boundary layer (i.e., the mixed layer) is represented by high q_T and high θ_E. Deep convection, which transports mixed layer air upward via pseudoadiabatic motions, conserves θ_E but reduces q_T by precipitation. Subsequent radiative cooling in the free troposphere decreases θ_E but conserves q_T. In tandem, these processes establish the low q_T, low θ_E values characteristic

[1]Cooperative Institute for Research in Environmental Sciences, Department of Atmospheric and Oceanic Sciences, University of Colorado Boulder, Boulder, Colorado, USA.
[2]Department of Atmospheric and Oceanic Sciences, University of Colorado Boulder, Boulder, Colorado, USA.

Corresponding author: A. Bailey, Cooperative Institute for Research in Environmental Sciences, University of Colorado Boulder, UCB 216, Boulder, CO 80309, USA. (adriana.bailey@colorado.edu)

2169-897X/13/10.1002/jgrd.50639

of air masses found at the top of the CBL. This free tropospheric air then mixes back into the boundary layer through entrainment, forming a transition layer characterized by a diagonal mixing line in q_T–θ_E space. *Betts and Albrecht* [1987] argued that the thermodynamic properties of the air mass at CBL top are particularly important in shaping the slope of this mixing line; however, their choice of tracers permitted only a cursory analysis of the origin of the dry end-member air mass.

[4] The present study revisits the conserved variable analysis of the CBL in order to evaluate bulk thermodynamic features of the transition layer and identify sources of moisture to the air masses that bookend it. In contrast with *Betts and Albrecht*'s [1987] work, the present analysis exploits stable isotope ratios in water as a tracer capable of distinguishing cloud processes and clear sky mixing. Because of saturation vapor pressure differences between heavy and light isotopologues, water vapor becomes depleted in isotopically heavy molecules during condensation and precipitation [*Bigeleisen*, 1961; *Dansgaard*, 1964]. As a result, stable isotope ratios in water help identify processes that moisten and dehydrate the atmosphere [*Worden et al*., 2007; *Noone*, 2012] and distinguish air masses by their integrated condensation histories [*Gat*, 1996].

[5] Various studies have used vapor isotope ratios to evaluate moist convective and mixing processes at multiple heights in the atmosphere. The departure of observed and simulated isotopic profiles from pseudoadiabatic models, for instance, suggests a role for lofting of frozen condensate by deep convection in moistening the upper troposphere [*Nassar et al*., 2007; *Bony et al*., 2008; *Blossey et al*., 2010; *Sayres et al*., 2010]. *Gedzelman* [1988] used isotope ratios in the lower and mid-free troposphere to distinguish air masses that had risen moist adiabatically but experienced different degrees of rainout and/or turbulent mixing. He also hypothesized that under certain advective conditions, free tropospheric air masses conserve their isotopic composition, providing a robust tracer of atmospheric motions. This finding has since been supported by large-scale advection models that reproduce, to first order, the isotope ratios observed in the subtropical free troposphere near Hawaii [*Galewsky et al*., 2007; *Hurley et al*., 2012]. In addition, *He and Smith* [1999] characterized moisture transport between the land surface and free atmosphere by pairing measurements of humidity and the stable isotope ratio in a simple mixing model.

[6] That isotope ratios distinguish air masses by their condensation histories and differentiate amongst moist convective and mixing processes enables the testing of several hypotheses regarding vertical moisture exchange in the subtropical CBL. We consider whether (1) the isotopic profile of the saturated mixed layer follows the Rayleigh distillation model predicted for pseudoadiabatic ascent, (2) the transition between mixed layer and free troposphere is accurately represented by a simple mixing process in terms of conserved isotopic variables, and (3) the top of the CBL is composed of free tropospheric air whose variations in isotope ratio are consistent with synoptic-scale transport. The desire to determine which processes control the isotopic composition of the air mass at CBL top builds on the expectation of *Betts and Albrecht* [1987] that this air mass critically influences mixing between the boundary layer and free troposphere.

[7] Vertical profile measurements of the water vapor mixing ratio (q) and the stable isotope ratio $^{18}O/^{16}O$ were made on the Big Island of Hawaii, 6–9 May 2010. Because of its remote Pacific setting and large vertical gain (~4200 m), the upper flanks of both Mauna Loa and Mauna Kea are exposed to free tropospheric air, while temperature and moisture at the island's lower elevations are typical of the subtropical marine boundary layer. This unique geographical and topographical setting makes it possible to sample the transition layer with high frequency and high spatial resolution using ground-based instrumentation [*Mendonca and Iwaoka*, 1969].

2. Methods

2.1. Instrumentation and Configuration of Sampling Platform

[8] Measurements of the water vapor mixing ratio (q), the oxygen and hydrogen isotope ratios, temperature, and submicron aerosol number size distributions were made during 6–9 May 2010 on the Big Island of Hawaii. Observed isotope ratios (*obs*) are reported in the δ notation relative to Vienna Standard Mean Ocean Water (*std*):

$$\delta D = \left(\frac{D/H_{obs}}{D/H_{std}} - 1\right) \times 1000 \quad (1)$$

$$\delta^{18}O = \left(\frac{^{18}O/^{16}O_{obs}}{^{18}O/^{16}O_{std}} - 1\right) \times 1000 \quad (2)$$

[9] Vertical profiles were obtained by driving from sea level to either the summit of Mauna Kea (~4200 m) or the Mauna Loa Observatory (~3400 m). Both the eastern and western sides of the island were profiled (Figure 1). Up to four profiles were driven each day, resulting in 12 profiles total. Because of nighttime driving restrictions near the astronomical observatory on Mauna Kea, 2 of the 12 profiles did not extend past the Mauna Kea Visitor Information Station (~2800 m). In addition, the last two profiles did not sample below the "Saddle," the height of land on Route 200, commonly called Saddle Road (~2000 m).

[10] The mixing ratio and isotope ratios were measured at 10 s frequency with a Picarro analyzer (the same instrument as *Noone et al*. [2013]), which uses cavity-enhanced tunable diode laser absorption spectroscopy (Picarro model 1115-i [*Gupta et al*., 2009]). Submicron aerosol was measured across 99 diameter ranges spanning 55–1000 nm using a Particle Metrics Ultra-High Sensitivity Aerosol Spectrometer (UHSAS, now sold by Droplet Measurement Technologies, Boulder, CO) [*Yokelson et al*., 2007; *Cai et al*., 2008]. Measurements of submicron aerosol number and size distributions were used to differentiate boundary layer and free tropospheric air masses and to assist in identification of cloud processes. Vehicle position and altitude were tracked with a Global Positioning System (GPS, Garmin model 60C). The Picarro and UHSAS were positioned inside the cab of a truck, and a 0.25 inch copper tube was strung through the rear passenger-side window for an inlet line. This line was nested inside a 1 inch schedule 80 polyvinylchloride (PVC) pipe, which was attached to the side of the vehicle to straighten the flow and reduce turbulence near the inlet. The inlet tip

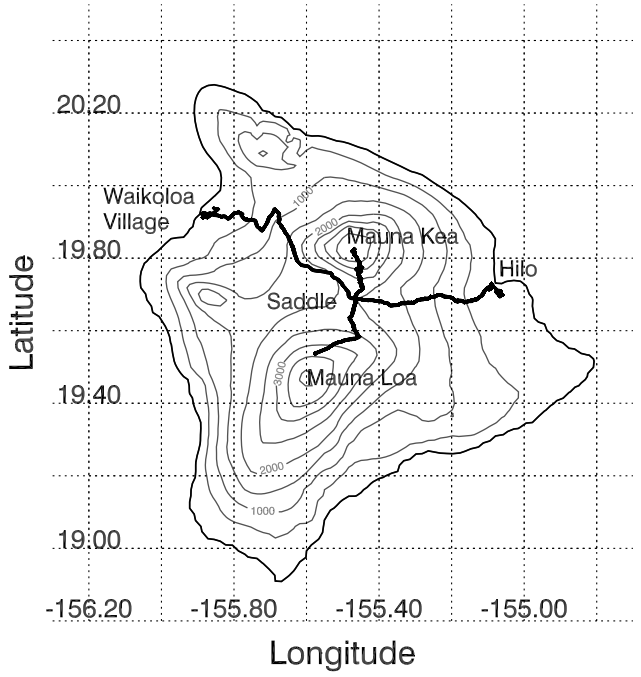

Figure 1. Map of the Big Island of Hawaii (topographic data source: *Amante and Eakins* [2009]). Profile starting and ending locations and driving routes measured by Global Positioning System (GPS) are marked as solid lines.

was angled backward to prevent rain drops and large debris from entering. Based on the pumping rate of the instruments, the flushing time of the inlet system was about 1 minute. (The elevation is not corrected for this time lag since the value is on the order of a few tens of meters, smaller than the error in the GPS-reported altitude.) A temperature probe was positioned within a second PVC pipe so that it was shielded from direct solar radiation. In addition, a LiCOR 7000 carbon dioxide and water vapor analyzer was operated to identify and exclude measurements affected by the exhaust of the truck and other vehicles on the road. The LiCOR measurements are not used otherwise or reported explicitly in this study.

[11] In practice, the Picarro instrument measures the total of all moisture, including small cloud droplets that evaporate within the sampling system. Consequently, the Picarro vapor mixing ratio measurements (q) should be nearly equivalent to the q_T measurements used by *Betts and Albrecht* [1987]. If the backward-facing inlet did reject some large cloud droplets, such a possibility does not critically change interpretation of the measurement. Indeed, *Albrecht et al.* [1979] suggested q is a reasonable approximation for q_T in conserved variable studies and much of the focus of this study is the unsaturated transition layer, where q and q_T are equal. Samples taken in rain and cloud are nevertheless flagged in the analysis for further discussion.

2.2. Isotopic Calibrations

[12] The isotopic measurements were calibrated to the Standard Mean Ocean Water–Standard Light Antarctic Precipitation (SMOW-SLAP) absolute isotopic scale [*Coplen*, 1994] using five secondary standards: Florida tap water; Boulder, Colorado tap water; water from West Antarctic Ice Sheet snow; water from Greenland snow; and water from surface snow from the Vostok drilling site in Antarctica. The isotopic values of these waters are shown in δ notation in Table 1. These secondary standards had been calibrated against International Atomic Energy Agency primary reference material on the University of Colorado Stable Isotope Laboratory's Isotope Ratio Mass Spectrometer (B. Vaughn, personal communication, 2010).

[13] Prior to field deployment, the secondary standards were measured on the vapor isotopic analyzer. A LEAP Technologies PAL (Prep and Load) autosampler was used to inject each standard by syringe into a Picarro vaporization module, which flash evaporated the liquid injection before delivery to the Picarro instrument. Although *Schmidt et al.* [2010] found some difference in the way Picarro vapor isotopic analyzers measure δD when the sample is liquid versus vapor, no significant difference was found in δ^{18}O. To reduce cross-contamination between standards, each standard was injected 15 times and isotope ratios from the last four injections were averaged to determine the final measurement. A known concentration bias in the Picarro vapor isotopic analyzers causes the instrument to measure isotope ratios differently at both very low and very high humidity [*Schmidt et al.*, 2010; *Tremoy et al.*, 2011; *Aemisegger et al.*, 2012]. To account for this, the five waters were sampled at up to seven mixing ratios (approximately 0.3, 0.6, 1.2, 2.4, 3.3, 6.5, and 11.9 g/kg) that were generated by controlling the amount of liquid injected into the vaporizer.

[14] Based on the 27 resulting calibration measurements, a locally weighted second-degree polynomial in two dimensions was used to characterize the isotopic bias relative to the absolute SMOW-SLAP scale in terms of both the isotope ratio and water vapor mixing ratio. The locally weighted surface was then used to predict isotopic biases for all combinations of isotope ratios and vapor mixing ratios measured in the field (Figures 2a–3a), and each field observation was corrected by subtracting its corresponding predicted bias. Standard errors from the prediction were used to characterize the uncertainty associated with the correction at each measurement point (Figures 2b–3b). At low humidity, such as observed on Mauna Kea's upper slopes, the isotopic bias can exceed 5.0 and 50.0 per mil in δ^{18}O and δD, respectively. The sign of the bias is instrument-specific and differs between the two isotope ratios, a finding consistent with previous studies [*Tremoy et al.*, 2011; *Aemisegger et al.*, 2012]. Simultaneously correcting the concentration bias and performing the isotopic calibration in this manner, rather than in the stepwise fashion adopted by previous studies [*Schmidt et al.*, 2010; *Tremoy et al.*, 2011; *Aemisegger et al.*, 2012; *Noone et al.*, 2013], was considered advantageous because it better accounts for covariation in measurement error in both humidity and isotope ratio, while avoiding the computational burden of Monte Carlo methods [cf. *Tremoy et al.*, 2011; *Noone et al.*, 2013].

Table 1. Isotope Ratio Values (per mil) of the Five Secondary Standards Used to Calibrate the Picarro Vapor Isotopic Analyzer

Standard Origin	δ^{18}O	δD
Florida	−0.56	−3.75
Boulder	−14.88	−113.06
West Antarctica	−26.11	−204.06
Greenland	−38.45	−300.74
Vostok	−56.13	−427.52

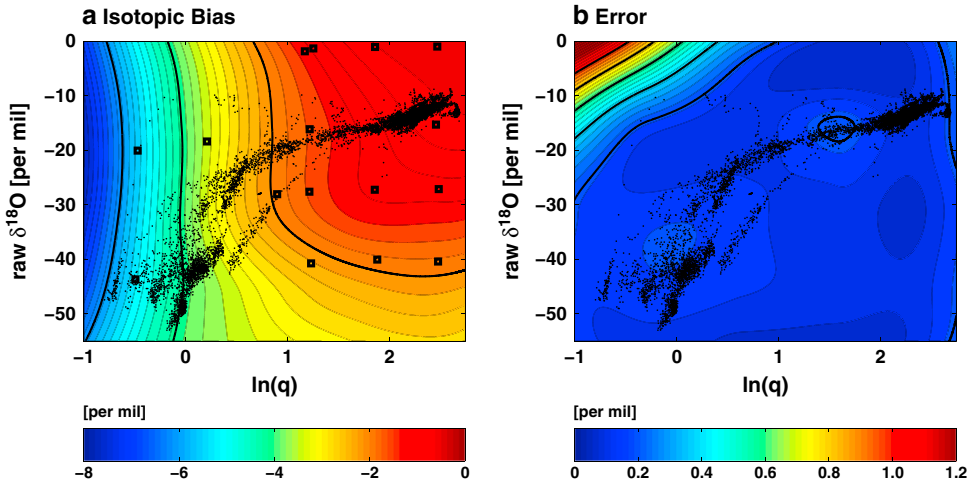

Figure 2. (a) The isotopic bias for raw δ^{18}O measurements and (b) the errors associated with the bias characterization (per mil) plotted as a function of both the raw isotopic value (per mil) and the natural log of the vapor mixing ratio (q) (g/kg). Contours are every 2.0 per mil in Figure 2a and 0.2 per mil in Figure 2b. The raw data (black dots) show the range of relevant biases. Nearby calibration points are represented by black squares in Figure 2a.

Nevertheless, the resulting analysis proves insensitive to subjective choices in the calibration procedure.

[15] The data set was further corrected by eliminating field measurements likely influenced by liquid water evaporation. These were identified by high values in either one isotope ratio or both. Since near-surface values are not the focus of this study, any measurements whose δD were higher than −60.0 per mil or whose δ^{18}O were higher than −6.0 per mil were simply excluded from the analysis. Similarly, a handful of extreme outliers, whose absolute deuterium excess exceeded three standard deviations of the deuterium excess mean (0.0 ± 17.0 per mil), were excluded. Figure 4 shows the effect of the calibration and data quality control procedures on the raw data. The large scatter is reduced, producing a linear regression of $\delta D = 7.02 \times \delta^{18}O - 18.48$ (with an uncertainty on the slope of ± 0.40 and an uncertainty on the intercept of ± 0.02). This result differs from the 8:1 relationship typical of precipitation globally [*Craig*, 1961; *Sharp*, 2007], as expected for tropical locations [*Dansgaard*, 1964].

[16] Additional biases due to day-to-day drift while measuring in the field were not quantified, due to the impracticality of operating a syringe injection system while driving on dirt roads; however, previous studies guide our expectation for drift. *Gupta et al.* [2009] found the same model Picarro instrument drifted by only 2.0 per mil in δD—equivalent to an approximate 0.25 per mil drift in δ^{18}O—over a four week period. Similarly, *Aemisegger et al.* [2012] detected a maximum drift in δ^{18}O of 0.5 per mil over a 14 day ambient sampling period. Therefore, to err on the side of caution, any differences in the corrected data less than 0.5 per mil in δ^{18}O are not considered significant.

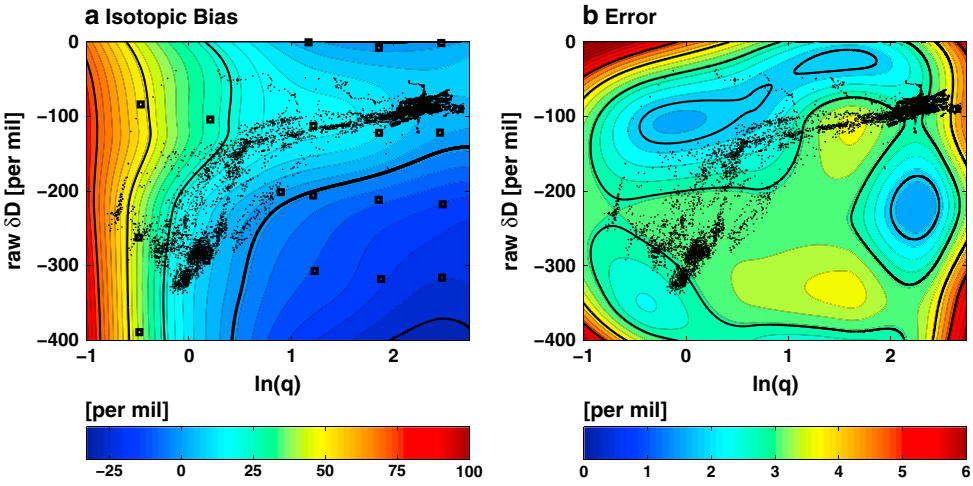

Figure 3. (a) The isotopic bias for raw δD measurements and (b) the errors associated with the bias characterization (per mil) plotted as a function of both the raw isotopic value (per mil) and the natural log of the vapor mixing ratio (q) (g/kg). Contours are every 25 per mil in Figure 3a , with the zero line bolded, and 5 per mil in Figure 3b. The raw data (black dots) show the range of relevant biases. Nearby calibration points are represented by black squares in Figure 3a.

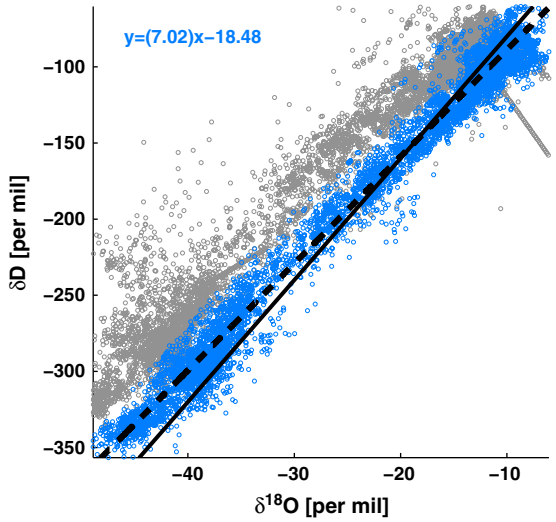

Figure 4. Raw (gray) and corrected (blue) isotopic data. The black line represents a meteoric water line with slope 8 and intercept 0. The dashed line is a simple linear regression fit to the corrected (blue) data.

[17] Sensitivity analyses were also conducted to evaluate the effects of instrument operating temperature and the time rate of ambient pressure change, caused by driving up and down the island, on the isotopic measurements. While the effects on δ^{18}O measurements were found to be negligible, effects on δD boundary layer measurements were evident for one profile. As a result, and because δD exhibits a slower response time to ambient changes (a larger "memory effect") and larger relative errors with calibration [*Schmidt et al.*, 2010; *Aemisegger et al.*, 2012], δ^{18}O measurements are used preferentially throughout the analysis.

2.3. Isotopic Models for the Convective Boundary Layer

[18] Due to differences in the saturation vapor pressures of heavy and light isotopologues of water [*Bigeleisen*, 1961], the relationship between the isotope ratio and observed vapor mixing ratio provides a valuable diagnostic for moisture fluxes [*Gat*, 1996; *He and Smith*, 1999; *Noone et al.*, 2011] and a means to distinguish moistening and dehydrating mechanisms [*Worden et al.*, 2007; *Noone*, 2012]. When conditions are unsaturated, both q and the isotope ratio are conserved variables, and airmass mixing will cause observations to fall along a line in δ–$1/q$ space [e.g., *He and Smith*, 1999; *Noone et al.*, 2011]. In contrast, if an air mass experiences a pseudoadiabatic process, in which condensate is immediately removed as precipitation, its δ value follows a theoretical Rayleigh distillation [e.g., *Dansgaard*, 1964]. By knowing q, temperature (T), and the heavy-to-light isotope ratio (R) at a certain height z_i and preceding height z_{i-1}, Rayleigh distillation predicts

$$R_i = R_{i-1}\left(\frac{q_i}{q_{i-1}}\right)^{\alpha-1} \tag{3}$$

where the subscripts i and i-1 denote two points along the upward distillation trajectory. If condensation is slow and thermodynamically reversible, α is the equilibrium fractionation factor, which determines the preferential removal of the heavy isotopes from the vapor phase as a function of T. T can be taken as the dew point temperature since q can be assumed at saturation during condensation. Furthermore, since all condensate is removed as precipitation, q is equivalent to q_T.

[19] To account for the presence of cloud within an adiabatic plume, the Rayleigh model may be modified so that conversion of condensate to precipitation is less than 100% [*Dansgaard*, 1964; *Jouzel and Merlivat*, 1984; *Noone*, 2012]. By defining a precipitation efficiency parameter ε, which varies from 0 if all condensate is held with the ascending vapor to 1 if all condensate is converted to precipitation, the isotope ratio of the vapor (R) can be written for discrete vertical points in the profile as

$$R_i = R_{i-1}\left(\frac{q_i + \alpha(1-\varepsilon)(q_0 - q_i)}{q_{i-1} + \alpha(1-\varepsilon)(q_0 - q_{i-1})}\right)^{\frac{\alpha\varepsilon}{1-\alpha(1-\varepsilon)}-1} \tag{4}$$

(e.g., *Noone* [2012], equation (11)). A limitation of this model, however, is the assumption that the vapor and liquid components of an air mass are always distinct. If the cloud liquid reevaporates at any point prior to observation or during sampling, as we expect was the case for our present experiment, then the isotope ratio measured will instead reflect a mixture of vapor and cloud. A better physical model for isotope ratio observations in the Hawaiian mixed layer is therefore given by a total water distillation (TWD) model:

$$R_T = (R_l l + Rq)/(l + q). \tag{5}$$

[20] Here, $l+q=q_T$ is the total water remaining in the air mass after precipitation. The cloud liquid at any height is given by $l=l_0+(1-\varepsilon)(q_0-q)$, where the subscript 0 denotes the value at some initial point, and the isotope ratio of the cloud (R_l) is simply a function of the equilibrium fractionation factor and the vapor isotope ratio predicted by equation (4) (i.e., $R_l=\alpha R$). Note that in the case of a pseudoadiabatic process (i.e., $\varepsilon=1$ and $l=0$), equation (5) reduces to $R_T=R$ and equation (4) reduces to the Rayleigh distillation model of equation (3).

[21] Figure 5 illustrates the expected dehydration and depletion pathways of subtropical air masses for the different moist convective and mixing processes described. If mixed layer air rises pseudoadiabatically into the free troposphere and all condensate immediately precipitates (i.e., $\varepsilon=1$), the $1/q$ and δ values of the transition layer will follow the dashed curve expected for Rayleigh distillation (equation (3)). If instead some condensate is held with the vapor in an adiabatic plume, total water isotope ratios will decrease less rapidly. The dotted curves show expected trajectories for air masses with precipitation efficiencies of 0.9 and 0.7. For a fully reversible moist adiabatic process, the total water and total water isotope ratio are conserved. On the other hand, if airmass mixing proves a better model for the vertical exchange of moisture between the boundary layer and free troposphere, then transition layer observations will form a straight line in the δ–$1/q$ space of the isotopic mixing diagram, similar to the q_T–θ_E mixing line described by *Betts and Albrecht* [1987].

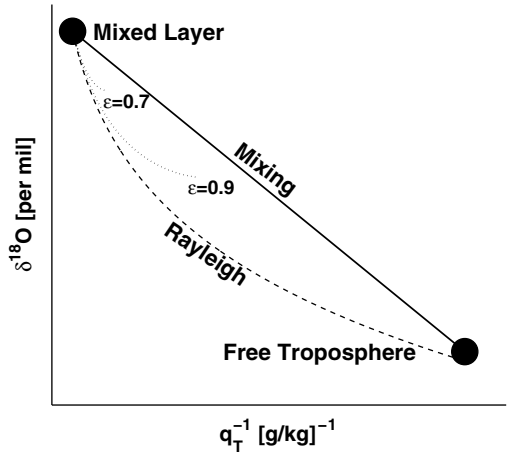

Figure 5. An isotopic mixing diagram of δ^{18}O versus the inverse of the total water mixing ratio (q_T). When mixed layer and free tropospheric air masses mix, observations fall along the straight (solid) line. Pseudoadiabatic processes result in Rayleigh distillation (dashed line), while moist adiabatic processes may follow one of the dotted lines, depending on their precipitation efficiency (ε). In a fully reversible moist adiabatic process ($\varepsilon = 0$), the total water and total water isotope ratio are conserved.

3. Results

3.1. Moisture Transport and Stratification Within the Mixed Layer

[22] To evaluate the processes regulating vertical moisture transport, we consider, in turn, moisture transport from the ocean surface to the top of the mixed layer and moisture transport from the top of the mixed layer, across the transition layer, to the top of the convective boundary layer (CBL). Ten vertical profiles of temperature, dew point temperature, and δ^{18}O are shown in Figure 6. Dew point temperature is derived from the Picarro q, with hydrostatic pressure estimated from the GPS altitude. Each profile is labeled according to its geographic starting and ending points (HI = Hilo, MK = Mauna Kea Visitor Information Station or Summit, ML = Mauna Loa Observatory, WV = Waikoloa Village) and for the day in May 2010 on which measurements were taken. For instance, the first profile is labeled MLHI6, since it was obtained on 6 May by driving from Mauna Loa Observatory to Hilo, on the eastern side of the Big Island. Arrows indicate whether the profile was measured by driving from lower to higher elevations, and thus moist to dry conditions, or vice versa. Moist adiabatic models (dashed blue lines, Figure 6) were chosen to fit the regions below the trade wind inversion in which temperature and dew point converged to within 0.5 K, except in the cases of the WVMK7 and MKWV8 profiles, which were fit in discrete segments. Before fitting, the data were binned using a 25 m average. Two additional half profiles were obtained on 9 May by driving from Mauna Kea to the Saddle (MKSA9) and from the Saddle to the Mauna Loa Observatory (SAML9).

3.1.1. Eastern Mixed Layer

[23] Mixed layer air is readily identifiable by the gradual decrease in temperature, dew point temperature, and δ^{18}O with height at altitudes below the level of the trade wind inversion; however, there are clear differences in humidity structure between the east and west sides of the island (Figure 6). On the east side of the island (represented by the six Hilo profiles), a single moist adiabat describes each dew point profile to first order (root mean square error < 1.0 K for the 500–2000 m layers of all but the HIMK7 profile). These findings are consistent with the expectation that easterly trade winds force air up the orographic rise, maintaining the profile near saturation. As a result, the east side exhibits higher humidity, higher precipitation totals, and lush vegetation, compared with the island's western slopes. A notable exception is the HIMK7 profile, in which dew point sharply decreases near 750 m and remains drier than the model adiabat to the Saddle at 2000 m. This discrepancy may result from nighttime stratification, since the profile was measured in the early hours before sunrise. Free air temperature measured by the Hilo radiosonde, launched at 0200 Hawaii-Aleutian Standard Time (HST), also indicates multiple weak stable layers below the inversion, which are no longer visible in the subsequent 1400 HST sounding (not shown).

[24] Isotopic measurements confirm the importance of moist adiabatic processes in controlling the vertical humidity structure of the mixed layer on the island's east side. Except for the MKHI7 profile, which was not modeled due to the lack of sufficient mixed layer isotope ratio data, isotopic profiles are matched by TWD models with precipitation efficiencies (ε) equal to or greater than 0.7. The HIMK8 profile is shown in Figure 7a as an example. Isotopic profiles were simultaneously fit above the lifting condensation level (LCL) using equation (5) and below the LCL using a constant isotope ratio. Variables allowed to vary in the fitting were the LCL height, the δ^{18}O value of the constant isotope ratio layer, and the precipitation efficiency (ε) in the layer of moist convection. The best parameters for each profile were selected by reducing the root mean square error of the fit for the 500–2000 m region. This region was selected to test adiabatic assumptions for each side of the island separately—since above 2000 m the east and west air masses may converge —and to avoid heavily trafficked areas near the coast.

[25] Though TWD models describe the eastern isotopic profiles to within 0.5 per mil root mean square error over the 500–2000 m region, above the Saddle (2000 m), isotopic observations diverge from the modeled adiabatic profiles over a short but significant vertical distance. The HIMK8 profile is a clear example (Figure 7a). In this profile, the δ^{18}O value increases above the Saddle before returning to the predicted adiabatic value at higher altitudes. Note that this departure from the predicted profile is distinct from the large decrease in δ^{18}O that occurs at 2700 m, associated with the transition to free tropospheric air. Instead, the layer of anomalously high δ^{18}O near the Saddle coincides approximately, but not exactly, with the altitudes where the vehicle passed through cloud (indicated by gray shading in Figures 6 and 7).

[26] The TWD model for the HIMK8 profile can be matched to the anomalous layer (2000–2300 m) to within 0.3 per mil root mean square error if the precipitation efficiency is lowered to 0.6 (Figure 7a). This finding suggests less condensate was removed from this layer as precipitation. Interestingly, the anomalously high δ^{18}O signal is observed before the vehicle enters the cloud, which suggests some of the condensate reevaporated within the Saddle region before the time of observation. Similar humidity "enhancements"

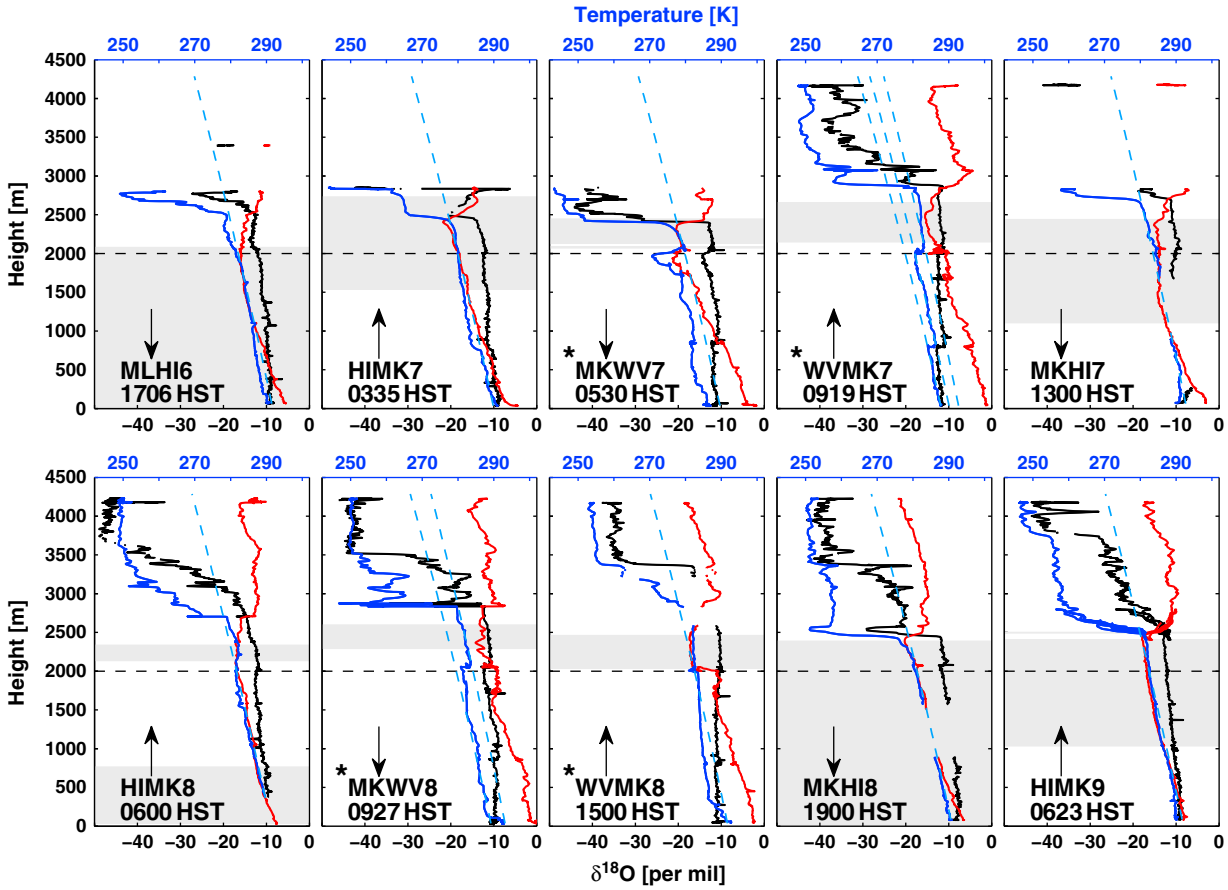

Figure 6. The first 10 profiles with temperature (red), dew point temperature (blue), and $\delta^{18}O$ (black) shown as a function of height. Modeled moist adiabats are shown as dashed blue lines. Arrows indicate the direction of profiling, and gray shading indicates regions where the vehicle passed through cloud or rain. The elevation of the Saddle (2000 m) is marked by the dashed black line. Profiles obtained from the island's dry west side are starred. Each profile is labeled according to its geographic starting and ending points (HI = Hilo, MK = Mauna Kea Visitor Information Station or Summit, ML = Mauna Loa Observatory, WV = Waikoloa Village) and for the day in May 2010 on which measurements were taken. For instance, the first profile is labeled MLHI6 because it was taken while driving from Mauna Loa Observatory to Hilo on 6 May. Each profile is also labeled with the time at which sampling began (profiles took approximately 2 hours to complete).

have been documented around isolated cumulus clouds [*Lu et al.*, 2003; *Laird*, 2005].

[27] If instead of using a TWD model, one considered a vapor-only model (equation (4)) for the HIMK8 profile, the predicted profile would fail to describe the 2000–2300 m layer no matter how much the precipitation efficiency were decreased. The yellow shading in Figure 7a shows the possible range of vapor isotope ratios predicted by equation (4) using the same LCL height and $\delta^{18}O$ value in the constant isotope ratio layer as selected for the best total water fit. To match a vapor model to the 2000–2300 m layer would require increasing either the LCL height or its $\delta^{18}O$ value, implying the anomalous air mass had lifted moist adiabatically at a different time or at a different location than the rest of the mixed layer profile. While these scenarios are certainly possible, the fact that air masses above, below, and within the anomalous layer can be explained by changing only the precipitation efficiency of the TWD model lends favor to the hypothesis that cloud reevaporation humidified the Saddle region.

[28] Thermodynamic boundaries within the HIMK8 profile can be assessed more readily by combining the $\delta^{18}O$ and q characteristics of the mixed layer in a $\delta^{18}O$–$1/q$ isotopic mixing diagram. The orange data points in Figure 8a, which correspond to the boxed section of the atmospheric profile shown in Figure 7a, suggest condensate reevaporation affects a deeper layer than Figure 7 indicates. The essential difference between these representations is that Figure 8 compares the adiabatic model with the isotope ratio and mixing ratio observations simultaneously, offering a more robust diagnostic of the water cycle histories of air masses than the isotope ratio alone.

3.1.2. Western Mixed Layer

[29] Because rainfall on the Big Island is chiefly controlled by orographic uplift and regional wind flow is predominantly easterly [*Price and Pales*, 1963], the mixed layer on the west side (the Waikoloa Village side) is climatologically drier than the mixed layer on the east side. As a result, western dew point temperature profiles from the May 2010 campaign exhibit greater stratification than the eastern profiles

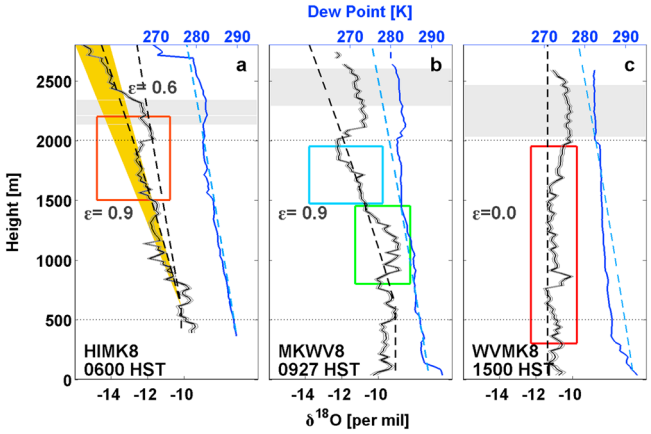

Figure 7. Isotope ratio profiles (solid black) with 1-σ envelope (solid gray) from three distinct profiles on 8 May: (a) HIMK8, (b) MKWV8, and (c) WVMK8. The best fit total water distillation models (dashed black) for the 500–2000 m layer (bounded by dotted lines) are shown with their precipitation efficiencies (ε). Dew point profiles (solid blue) and moist adiabatic models (light blue dashed) are also shown for reference. Regions where the vehicle drove through cloud are shaded light gray. Yellow shading in Figure 7a indicates the range of possible vapor-only models. The boxed regions are discussed in the text.

(Figure 6). Stable stratification is particularly evident in the early morning MKWV7 profile, whose dew point temperature, ambient temperature, and δ^{18}O all decrease significantly in the layer below the Saddle. Although stratification persists and relative humidity remains low in mid-morning profiles WVMK7 and MKWV8, their dew point temperatures follow moist adiabatic lapse rates within discrete stable layers. (Figure 7b shows this in greater detail for the MKWV8 profile.) Such observations indicate a recent history of condensation and perhaps point to the east side as the origin of these air masses. Indeed, wind fields around the Big Island provide a possible explanation for how eastern air masses may be transported to the west side: while the easterly trade winds split around the mountain barrier [*Leopold*, 1949; *Garrett*, 1980], turbulent vortices on the lee side cause easterly flowing air to reverse direction back toward the western coast [*Yang et al*., 2008]. Furthermore, air masses that lose some condensate through precipitation—whether on the "rainy" east side or in another saturated environment—should preserve their adiabatic signature as they advect into the warmer, drier environment of the island's west coast, so long as they are not turbulently mixed. The western observations thus clearly show that moist convection influences the humidity structure of even the unsaturated regions of the mixed layer.

[30] Differences in aerosol size distributions between the east and west sides of the island further support the idea that moist convection sets the humidity structure of the west side. When a cloud evaporates, aerosol particle sizes should increase if droplets have been processed within the cloud, for example by coalescence [*Hoppel et al*., 1986]. While aerosol number size distributions in the eastern mixed layer were always unimodal (within the detectable 55–1000 nm size range) with mean number diameters of ~130 nm (Figure 9), size distributions on the west side were frequently bi- or trimodal, exhibiting a pronounced mode at larger diameters (mean number diameters of ~300 nm) (Figure 9c). (Note that the measured aerosol diameters are distinctly larger than the marine boundary layer aerosol reported by *Hoppel et al*. [1986] in part because the aerosols were not dried prior to sampling by the UHSAS.) In the MKWV8 profile, for instance, the aerosol size distribution shows the pronounced 300 nm mode (blue shading, Figure 9c) where the isotopic profile is moist adiabatic (1450–1950 m, blue box, Figure 7b)—a finding consistent with the supposition that cloud droplets had coalesced before evaporating prior to observation—but is unimodal (green shading, Figure 9b) where the constant isotope ratio with height indicates the boundary layer is fully mixed (800–1450 m, green box, Figure 7b). The δ^{18}O–1/q mixing diagram, shown in Figure 8b, confirms that these adjacent sections of the profile are indeed distinct air masses.

[31] Once wind speed and dry turbulent mixing increased during the afternoon of 8 May, the partly stratified

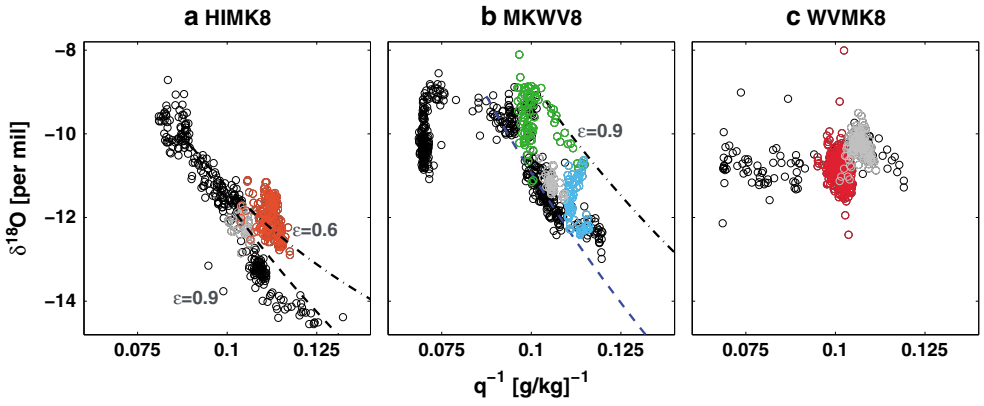

Figure 8. Isotopic mixing diagrams of the three mixed layer profiles shown in Figure 7: (a) HIMK8, (b) MKWV8, and (c) WVMK8. In-cloud observations are shaded light gray. Orange, green, blue, and red shading correspond to the boxed sections of Figure 7. Modified distillation models with different precipitation efficiencies (ε) (dashed black) are shown in Figures 8a and 8b. The blue dashed line in Figure 8b represents a hypothetical Rayleigh distillation that passes through the cloudy layer above the Saddle.

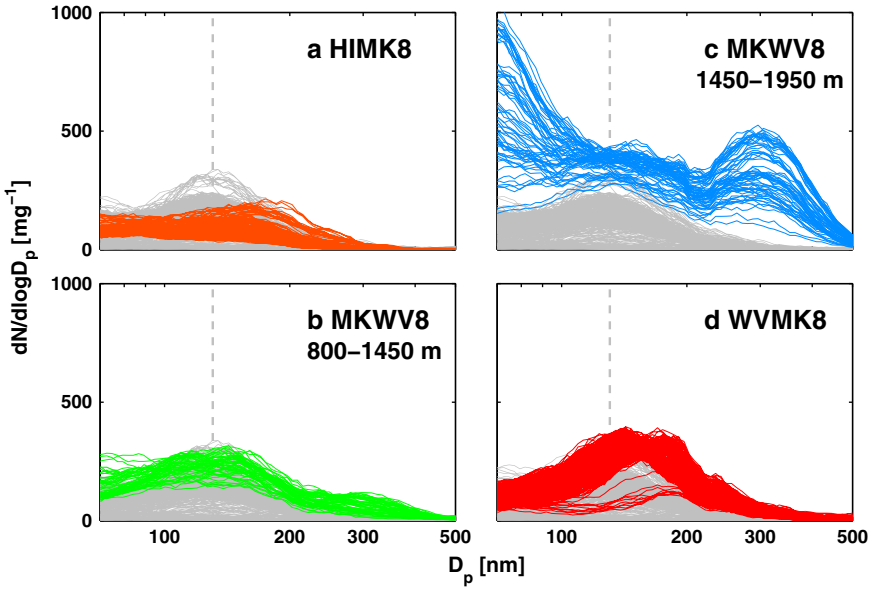

Figure 9. Aerosol number size distributions with five bin smoothing corresponding to the profile sections marked with boxes in Figure 7: (a) HIMK8, (b) MKWV8 lower profile, (c) MKWV8 upper profile, and (d) WVMK8. For comparison, aerosol size distributions sampled from the mixed layer of the east side of the island on 7 and 9 May are shown in light gray and their mean size (130 nm) is marked by the gray dashed lines.

MKWV8 profile was replaced by a constant isotopic profile (WVMK8, Figure 7c) and the disparate air masses highlighted on the isotopic mixing diagram were replaced by a single cluster of points (Figure 8c). Similarly, a unimodal aerosol size distribution was observed along the length of the mixed layer profile, including where a multimodal distribution had existed earlier (Figure 9d). These results suggest that because paired humidity and isotope ratio measurements distinguish atmospheric layers shaped by different moist convective and turbulent mixing processes, they can provide physical explanations for changes in aerosol observed. They also imply cloud reevaporation and dry turbulent mixing can influence the humidity and isotopic composition of the base of the transition layer. A traditional Rayleigh model is therefore insufficient for characterizing moisture transport from the ocean surface to the top of the Hawaiian mixed layer; it cannot account for the discrete regions of airmass mixing observed.

3.2. Airmass Mixing Within the Transition Layer

[32] Having established several mechanisms that influence the humidity and isotopic composition of the mixed layer, we now turn to evaluating the interaction between the mixed layer and free troposphere. Above the trade wind temperature inversion, the Hawaii dew point profiles clearly diverge from the moist adiabatic lapse rate and stabilize at very low values near the Mauna Kea summit (~4200 m) (Figure 6). If moist convection were the dominant process transporting moisture above the inversion and into the lower free troposphere, the dew point temperature and $\delta^{18}O$ should track the modeled moist adiabats and modified distillation models through the transition layer. Instead, both humidity and $\delta^{18}O$ decline much more rapidly, as one might expect when mixing with very dry and depleted free tropospheric air occurs.

[33] To test whether mixing is indeed the best model for moisture exchange between the boundary layer and free troposphere, the isotope ratio is plotted against the inverse of the vapor mixing ratio, and straight-line segments are identified. Figure 10 shows observations from nine of the first 10 profiles plotted on such an isotopic mixing diagram. The HIMK7 profile is excluded due to extensive inlet wetting when the vehicle passed through cloud.

[34] Contrary to expectation, in most profiles, the region between the top of the mixed layer and the Mauna Kea summit (i.e., the driest and most depleted free tropospheric observations) is not well described by a single mixing line. Instead, the data are often characterized by bent-line structures, composed of multiple, adjoining straight-line segments. The approximate boundary between these segments is

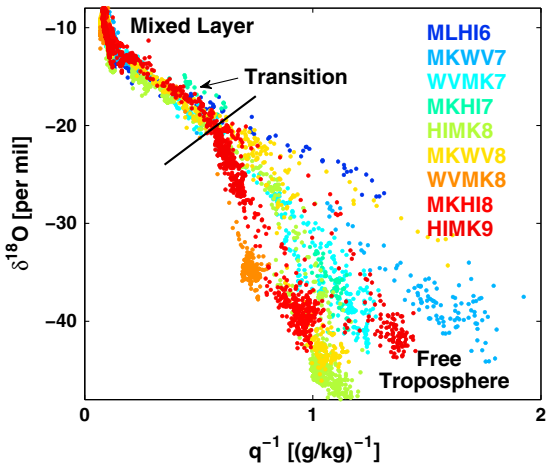

Figure 10. An isotopic mixing diagram for nine profiles. The transition layer is represented by the straight-line segments that lie largely to the left of the black line. Mauna Kea summit air masses are represented by the dry and isotopically depleted clusters to the right of the black line.

Table 2. Coefficients of Determination (r^2) and Number of Points (n) Used in Regressing the $\delta^{18}O$ on $1/q$ for the Transition Layers of the Bent-Line Profiles Shown in Figure 10

Profile	r^2	n
MKHI7	0.91	23
HIMK8	0.98	149
MKWV8	0.96	203
WVMK8	- - -	0
MKHI8	0.96	21
HIMK9	0.81	123

marked by a solid black line in Figure 10; however, the exact location is profile-dependent.

[35] Straight-line segments to the left of the black line, in the region linking the top of the mixed layer with the free tropospheric air above the trade wind temperature inversion, are well described by simple linear regressions that are significant at the 0.01 level (Table 2). (Observations from the top of the mixed layer were not included in the regressions to avoid inflating the r^2 values.) Such high coefficients of determination confirm that mixing is a suitable model for vertical moisture exchange across the transition layer. In contrast, the line segments to the right of the black line are not as well defined since they appear to represent vertical layering of free tropospheric air masses. Aerosol number size distributions provide supporting evidence. Within the transition layer, aerosol number size distributions span large ranges in number concentration, as might be expected with dilution or mixing (Figure 11). Above the transition layer (to the right of the black line), aerosol populations appear distinct and undiluted, as would be expected for distinct free tropospheric air masses.

[36] Importantly, the isotopic mixing diagram shows that when the atmospheric profile above the mixed layer is characterized by a bent-line structure, the air at the top of the transition layer—the top of the CBL—is not the same air mass as that observed at the Mauna Kea summit. Variations in the vapor mixing ratio and $\delta^{18}O$ of these distinct air masses reflect the diverse processes that regulate their thermodynamic properties.

3.3. Processes Influencing the Moisture Properties at CBL Top

[37] Over the course of the four day field campaign, the free tropospheric air near the Mauna Kea summit experienced large relative changes in humidity and isotope ratio. On hourly time scales, local vertical motions may have influenced the q and $\delta^{18}O$ properties of this air mass. Close inspection of consecutive profiles HIMK8, MKWV8, WVMK8, and MKHI8, for instance, suggests variations in the summit air mass (isotopic range: −45.5 to −34.8 per mil) aligned with a single vertical mixing line whose moist end-member was the subtropical mixed layer (Figure 10). On daily time scales, however, q–$\delta^{18}O$ variability did not follow the same mixing pattern. Nor was it consistent with modified distillation expected during moist convection (refer to Figure 5). Instead, large variations along the x axis in the isotopic mixing diagram (Figure 10) point to a probable role for large-scale transport, which previous studies have argued controls the isotopic composition of the free troposphere near Hawaii to first order [*Galewsky et al.*, 2007; *Noone et al.*, 2011; *Hurley et al.*, 2012].

[38] Notably, the large variations in q and $\delta^{18}O$ near the Mauna Kea summit had little effect on the air mass at CBL top. Variability in the latter was instead narrowly confined to the mixing line that defines the Hawaii transition layer, a behavior that suggests vertical mixing with the boundary layer influenced the q and $\delta^{18}O$ properties of this air mass. The MKWV7 profile, for example, is the last profile in Figure 10 to exhibit a single straight-line structure. During subsequent profiles, the CBL top simply moves up and down the original MKWV7 mixing line, even as variations in air masses at higher elevation cause the "bend" to form on the isotopic mixing diagram. These findings suggest entrainment-

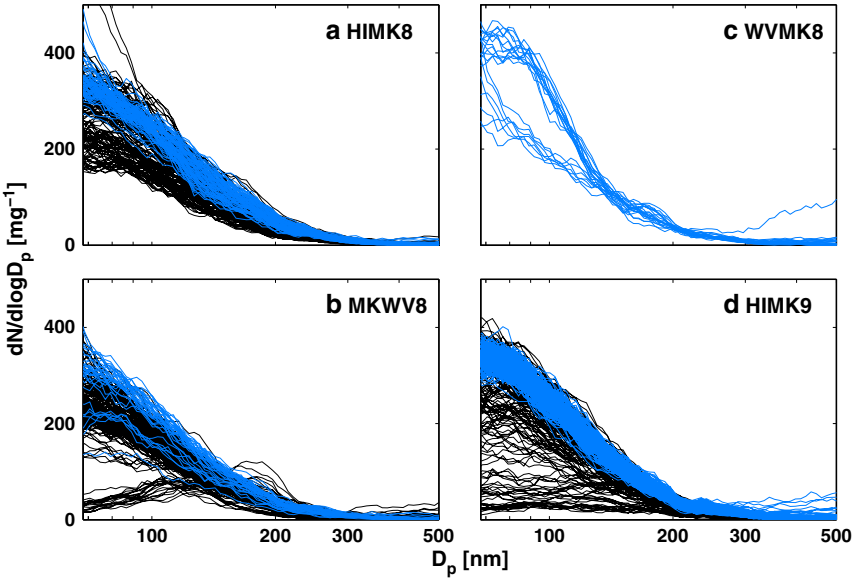

Figure 11. Aerosol number size distributions with five bin smoothing representing the transition layer (black) and free troposphere above (blue) for profiles (a) HIMK8, (b) MKWV8, (C) WVMK8, and (d) HIMK9.

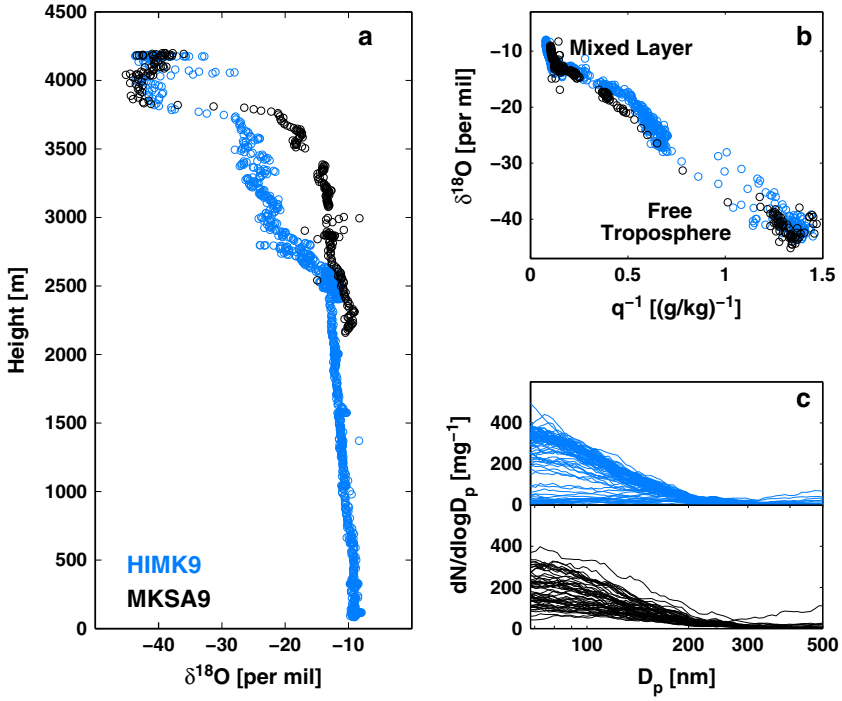

Figure 12. (a) Isotopic profiles for the HIMK9 (blue) and MKSA9 (black) profiles, whose transition layers were observed at approximately 0830 and 1000 HST, respectively, on 9 May (b) On an isotopic mixing diagram, the HIMK9 profile shows a bent-line structure above the mixed layer while the MKSA9 profile is represented by a single straight line. (c) Their respective aerosol number size distributions (with 5 bin smoothing) in the 2500–3700 m layer.

mixing on 7 May set the q–$\delta^{18}O$ composition of the air mass at CBL top, which then persisted as a residual layer through the morning of 9 May. While vertical mixing remained weak during this period, the boundary layer would have entrained air from the residual layer rather than from the free troposphere above. Entrainment feedbacks on surface moisture and heat fluxes would have thus occurred in isolation of the free tropospheric changes driven by large-scale transport.

[39] The development of strong convective mixing on 9 May eliminated evidence of the residual layer in the MKSA9 profile by resetting the thermodynamic structure of the transition layer. Figure 12 compares the MKSA9 profile (transition layer observed ~1000 HST) with the preceding HIMK9 profile (transition layer observed ~0830 HST); the MKSA9 profile shows a clear deepening of the transition layer by a full kilometer (Figure 12a). All observations above the mixed layer shift from a bent line to a straight line on the isotopic mixing diagram, and clustering of these points near the moist end-member indicates dramatic humidification and enrichment of the upper slopes of Mauna Kea (Figure 12b). Changes in aerosol number size distributions are also consistent with stronger mixing and transition layer deepening (Figure 12c). During the early morning ascent of Mauna Kea (HIMK9), aerosol within the 2500–3700 m layer of the atmosphere was characterized by two largely distinct populations. By the time of the return trip down the mountain (MKSA9), a single gradient in number concentration was observed across this same vertical range.

[40] Changes in wind profiles provide a possible physical explanation for the stronger mixing indicated by the isotope and aerosol data. The trade wind temperature inversion typically limits convective activity on Hawaii's east side [*Price and Pales*, 1963; *Garrett*, 1980]; however, *Noone et al*. [2011] observed strong convective activity when regional winds shifted to southwesterly. Upper air radiosondes

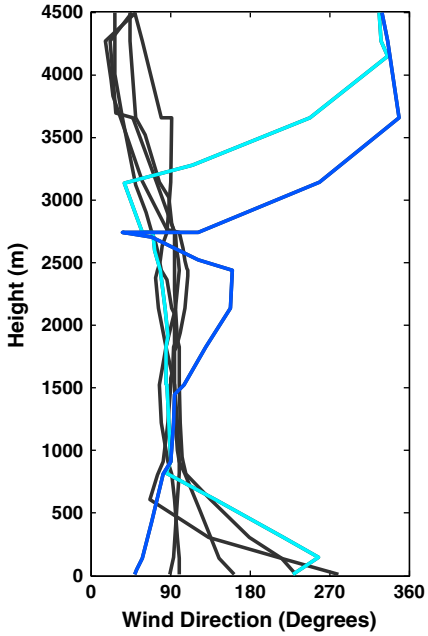

Figure 13. Wind direction as a function of height from the Hilo radiosondes for 6–9 May 2010. The aqua and blue profiles are the last two profiles for the period, launched at 0200 and 1400 HST, respectively, on 9 May.

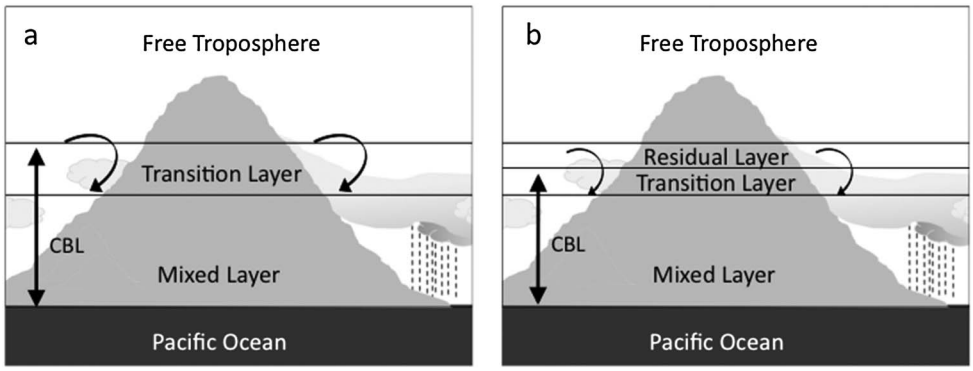

Figure 14. Two possible representations of the lower atmosphere near Hawaii (not to scale). (a) The convective boundary layer (CBL) entrains air directly from the free troposphere, producing a single straight line on an isotopic mixing diagram (see Figures 5 and 10). (b) When convective mixing is not as strong, the CBL entrains air from a residual layer formed during previous boundary layer growth. Weaker mixing, combined with free tropospheric advection, produces a bent-line structure on an isotopic mixing diagram.

from Hilo show a clear westerly shift in the upper level wind direction on 9 May (Figure 13), which may have facilitated convective development throughout the morning. Though one coincident observation of a well-developed transition layer and a shift in upper level winds cannot test causality between regional windflow and local convection, it nevertheless suggests future work should consider the effect of large-scale conditions in shaping entrainment-mixing and in setting the moisture properties of the residual layer that forms at CBL top.

4. Discussion

[41] *Betts and Albrecht* [1987] suggested the dry air mass at CBL top was critical in determining the thermodynamic structure of mixing between the boundary layer and free troposphere. Our study affirms this hypothesis and also suggests the mixing process, in turn, influences the moisture properties of CBL top. In the MKWV7 and MKSA9 profiles, a single mixing line in $\delta^{18}O$–$1/q$ space was observed to link the top of the mixed layer with the free tropospheric air near Mauna Kea. The slope of the CBL mixing line was therefore directly influenced by the isotopic composition of Hawaii's free troposphere (Figure 14a), which previous studies suggest is controlled to first order by large-scale transport [*Galewsky et al*., 2007; *Noone et al*., 2011; *Hurley et al*., 2012]. In contrast, beginning with the WVMK7 profile and lasting until the HIMK9 profile, the top of the CBL was capped by a residual layer, whose isotopic composition had been influenced by previous mixing with the boundary layer (Figure 14b). These results imply that moisture properties at the top of the Hawaiian CBL can be set either by large-scale free tropospheric transport or by vertical mixing initiated by boundary layer convection. Assumptions that large-scale transport alone is responsible for the low humidity of the subtropical atmosphere clearly fail to account for the possible role of local vertical processes in moistening the climatically important free troposphere.

[42] Whether or not residual layers cap the CBL appears to depend on the strength of entrainment-mixing. In the MKSA9 profile, strong convection caused a deep entrainment zone to develop, linking the top of the mixed layer with the free tropospheric air near the island's summit. As all evidence of the residual layer vanished, upper level winds concurrently shifted direction, suggesting a possible connection between free tropospheric dynamics and the strength of convection. Indeed, such a correlation is well supported by previous studies. While the trade wind inversion regulates convective strength on the Big Island [*Price and Pales*, 1963; *Garrett*, 1980], *Cao et al*. [2007] showed that synoptic conditions regulate the inversion. *Mendonca* [1969] further showed that stronger trade winds favor stronger convection on Hawaii. Yet it remains unclear whether changes in large-scale wind patterns are central to climatological moisture transport across the inversion layer. For this reason, testing the sensitivity of convective mixing to free tropospheric dynamics using a longer isotopic observational data set would be an important direction for future study.

[43] There are two principle reasons isotopic "tracers" successfully track entrainment-mixing: their dynamic range at low humidity and their lifetime. The former makes it possible to differentiate air masses that have undergone unique dehydration histories despite being indistinguishable in terms of their vapor mixing ratios. On 8 May, for instance, there were times when the vapor mixing ratio at the top of the CBL was nearly identical to the vapor mixing ratio of the free tropospheric air near the Mauna Kea summit (Figure 10). Only in considering the isotope ratio was the CBL top identified as a distinct residual layer. Detection of this residual layer was also possible because vapor isotope ratios are conserved in the free troposphere unless altered by convective mixing or large-scale transport, precisely the processes expected to break up residual layers. Were isotope ratios characterized by a much longer time scale, the CBL top would tend toward a uniform $\delta^{18}O$ value. A shorter time scale and the isotopic signature of the residual layer would not persist from one day to the next.

[44] In addition to characterizing the dry air mass at CBL top, isotope ratios provide valuable information about the processes that shape the moist air mass at the base of the transition layer. Using a total water distillation (TWD) model (in which the amount of condensate converted to precipitation is allowed to vary), adiabatic processes with different precipitation efficiencies were identified below the trade wind

temperature inversion. Interestingly, a single ε value was not always sufficient for describing adjacent sections of the same profile. In the HIMK8 mixed layer profile, for instance, adjacent layers were described by two distinct adiabatic models, with the lower precipitation efficiency model ($\varepsilon = 0.6$) matching the layer in which cloud reevaporation had likely occurred (Figure 8a). Although $\varepsilon = 0.6$ produced the best fit for this layer, a model with $\varepsilon = 0.7$ would have also produced a root mean square error less than 0.3 per mil. To distinguish amongst such models statistically, it will be necessary to reduce uncertainties in vapor isotope ratio measurements below 0.5 per mil. Fortunately, rapid advancement in commercial isotope ratio measurement technologies has already resulted in substantial improvements in measurement precision.

[45] One important remaining consideration is whether results from Hawaii may be extrapolated to the subtropics generally. Undoubtedly, radiative heating of the land during the day enhances convective development on the island compared to the neighboring open ocean. Mechanical lifting may also cause air masses to slide upslope, creating an apparent CBL deepening due to the fact that ground-based measurements do not follow a truly vertical axis. For example, this study's in situ measurements identified the sharp changes in vapor mixing ratio and ambient temperature that mark the trade wind inversion as occurring at higher altitudes than free atmospheric measurements made by radiosonde indicate. *Mendonca and Iwaoka* [1969] found similar height differences between their on-island ground-based temperature measurements and off-island balloon soundings. Yet because such discrepancies primarily affect the absolute depths of the CBL and its transition layer, they are not necessarily relevant to the objectives of this study. Rather, the idea that vertical mixing processes observed on Hawaii are representative of the subtropics generally is demonstrated by the qualitative similarities between this work and the work of *Betts and Albrecht* [1987], whose data set applies much more broadly to the tropical/subtropical region. In both studies, the transition layer near CBL top is characterized as a mixing line linking two distinct humidity regimes: the ocean-moistened mixed layer and the dehydrated free troposphere.

5. Conclusion

[46] This study has used stable isotope ratios in water to investigate processes that facilitate moisture transport from the ocean surface into the lower free troposphere near the Big Island of Hawaii. Below the trade wind temperature inversion, daytime isotopic profiles on the island's east side were always consistent with a moist adiabatic model of convection. Western profiles, in comparison, exhibited a range of stratification that varied daily, as well as evidence of dry turbulent mixing. Isotope ratios helped distinguish the influence of cloud processes and mixing on water vapor within the CBL, providing physical explanations for the dramatic differences in aerosol number size distributions observed. Moreover, since accounting for cloud condensate reevaporation was important for explaining the isotope ratios measured near the top of the mixed layer, Rayleigh distillation proved inadequate for describing moisture transport within the Hawaiian boundary layer.

[47] In contrast, moisture transport between the boundary layer and free troposphere was best characterized by a vertical mixing model, whose solution plots as a straight line in the $\delta^{18}O$–$1/q$ space of an isotopic mixing diagram. Deviations from the straight-line fit identified boundaries in the thermodynamic structure of the atmospheric profiles, marking, for example, residual layers that had formed during previous mixing events. Such residual layers capped the CBL in more than half the profiles sampled. During these periods, basic assumptions that synoptic-scale transport controls the air mass at CBL top were not sufficient for characterizing the vertical exchange of moisture in the lower subtropical atmosphere. Instead, it was the residual layer that shaped the mixing-line structure of the transition layer. Since strong mixing events likely set the residual layers that influence vertical mixing for multiple days at a time, understanding the factors that control the strength of convection is an important next step for predicting changes in vertical moisture transport between the subtropical boundary layer and free troposphere.

[48] **Acknowledgments.** This work was supported by a fellowship from the Department of Atmospheric and Oceanic Sciences, University of Colorado Boulder, a National Science Foundation Graduate Research Fellowship, a grant from the NASA Jet Propulsion Laboratory, the National Science Foundation Early Career and Climate and Large-scale Dynamics programs (AGS-0955841), and funds from the Cooperative Institute for Research in Environmental Sciences. We thank Balaji Rajagopalan at the University of Colorado Boulder for guidance in developing the locally weighted regression model used in calibrating the isotope ratio data.

References

Aemisegger, F., P. Sturm, P. Graf, H. Sodemann, S. Pfahl, A. Knohl, and H. Wernli (2012), Measuring variations of $\delta^{18}O$ and $\delta^{2}H$ in atmospheric water vapour using two commercial laser-based spectrometers: An instrument characterisation study, *Atmos. Meas. Tech.*, *5*, 1491–1511.

Albrecht, B. A., A. K. Betts, W. H. Schubert, and S. K. Cox (1979), Model of the thermodynamic structure of the trade-wind boundary layer: Part I. Theoretical formulation and sensitivity tests, *J. Atmos. Sci.*, *36*, 73–89.

Amante, C., and B. W. Eakins (2009), *ETOPO1 1 Arc-Minute Global Relief Model: Procedures, Data Sources and Analysis*, NOAA Technical Memorandum NESDIS NGDC-24, 19 pp., NOAA NGDC, Boulder, Colorado.

Ayotte, K. W., et al. (1996), An evaluation of neutral and convective planetary boundary-layer parameterizations relative to large eddy simulations, *Boundary-Layer Meteorol.*, *79*, 131–175.

Betts, A. K., and B. A. Albrecht (1987), Conserved variable analysis of the convective boundary layer thermodynamic structure over the tropical oceans, *J. Atmos. Sci.*, *44*, 83–99.

Bigeleisen, J. (1961), Statistical mechanics of isotope effects on the thermodynamic properties of condensed systems, *J. Chem. Phys.*, *34*, 1485–1493.

Blossey, P. N., Z. Kuang, and D. M. Romps (2010), Isotopic composition of water in the tropical tropopause layer in cloud-resolving simulations of an idealized tropical circulation, *J. Geophys. Res.*, *115*, D24309 doi:10.1029/2010JD014554.

Bony, S., C. Risi, and F. Vimeux (2008), Influence of convective processes on the isotopic composition (d18O and dD) of precipitation and water vapor in the tropics: 1. Radiative-convective equilibrium and Tropical Ocean-Global Atmosphere-Coupled Ocean-Atmosphere Response Experiment (TOGA-COARE) simulations, *J. Geophys. Res.*, *113*, D19305 doi:10.1029/2008JD009942.

Bretherton, C. S., P. Austin, and S. T. Siems (1995), Cloudiness and marine boundary layer dynamics in the ASTEX Lagrangian experiments. Part II: Cloudiness, drizzle, surface fluxes, and entrainment, *J. Atmos. Sci.*, *52*, 2724–2735.

Brooks, I. M., and A. M. Fowler (2012), An evaluation of boundary-layer depth, inversion and entrainment parameters by large-eddy simulation, *Boundary-Layer Meteorol.*, *142*, 245–263, doi:10.1007/s10546-011-9668-3.

Cai, Y., D. C. Montague, W. Mooiweer-Bryan, and T. Deshler (2008), Performance characteristics of the ultra high sensitivity aerosol spectrometer for particles between 55 and 800 nm: Laboratory and field studies, *J. Aerosol Sci.*, *39*, 759–769.

Cao, G., T. W. Giambelluca, D. E. Stevens, and T. A. Schroeder (2007), Inversion variability in the Hawaiian trade wind regime, *J. Clim.*, *20*, 1145–1160.

Coplen, T. B. (1994), Reporting of stable hydrogen, carbon, and oxygen isotopic abundances, *Pure Appl. Chem.*, *66*, 273–276.

Craig, H. (1961), Isotopic variations in meteoric waters, *Science*, *133*, 1702–1703.

Dansgaard, W. (1964), Stable isotopes in precipitation, *Tellus*, *16*, 436–468.

Deardorff, J. W., G. E. Willis, and B. H. Stockton (1980), Laboratory studies of the entrainment zone of a convectively mixed layer, *J. Fluid Mech.*, *100*, 41–64, doi:10.1017/S0022112080001000.

Faloona, I., D. H. Lenschow, T. Campos, B. Stevens, M. van Zanten, B. Blomquist, D. Thornton, A. Bandy, and H. Gerber (2005), Observations of entrainment in Eastern Pacific marine stratocumulus using three conserved scalars, *J. Atmos. Sci.*, *62*, 3268–3285, doi:10.1175/JAS3541.1.

Galewsky, J., M. Strong, and Z. D. Sharp (2007), Measurements of water vapor D/H ratios from Mauna Kea, Hawaii, and implications for subtropical humidity dynamics, *Geophys. Res. Lett.*, *34*, L22808, doi:10.1029/2007GL031330.

Garrett, A. J. (1980), Orographic cloud over the eastern slopes of Mauna Loa volcano, Hawaii, related to insolation and wind, *Mon. Weather Rev.*, *108*, 931–941.

Gat, J. R. (1996), Oxygen and hydrogen isotopes in the hydrologic cycle, *Annu. Rev. Earth Planet. Sci.*, *24*, 225–262.

Gedzelman, S. D. (1988), Deuterium in water vapor above the atmospheric boundary layer, *Tellus*, *40B*, 134–147.

Gupta, P., D. Noone, J. Galewsky, C. Sweeney, and B. H. Vaughn (2009), Demonstration of high-precision continuous measurements of water vapor isotopologues in laboratory and remote field deployments using wavelength-scanned cavity ring-down spectroscopy (WS-CRDS) technology, *Rapid Commun. Mass Spectrom.*, *23*, 2534–2542.

He, H., and R. B. Smith (1999), Stable isotope composition of water vapor in the atmospheric boundary layer above the forests of New England, *J. Geophys. Res.*, *104*, 11,657–11,673.

Hoppel, W. A., G. M. Frick, and R. E. Larson (1986), Effect of nonprecipitating clouds on the aerosol size distribution in the marine boundary layer, *Geophys. Res. Lett.*, *13*, 125–128.

Hu, X.-M., J. W. Nielsen-Gammon, and F. Zhang (2010), Evaluation of three planetary boundary layer schemes in the WRF model, *J. Appl. Meteorol. Climatol.*, *49*, 1831–1844.

Hurley, J. V., J. Galewsky, J. Worden, and D. Noone (2012), A test of the advection- condensation model for subtropical water vapor using stable isotopologue observations from Mauna Loa Observatory, Hawaii, *J. Geophys. Res.*, *117*, D19118, doi:10.1029/2012JD018029.

Jouzel, J., and L. Merlivat (1984), Deuterium and oxygen 18 in precipitation: Modeling of the isotopic effects during snow formation, *J. Geophys. Res.*, *89*, 11,749–11,757.

Laird, N. F. (2005), Humidity halos surrounding small cumulus clouds in a tropical environment, *J. Atmos. Sci.*, *62*, 3420–3425.

Lenschow, D. H., P. B. Krummel, and S. T. Siems (1999), Measuring entrainment, divergence, and vorticity on the mesoscale from aircraft, *J. Atmos. Oceanic Technol.*, *16*, 1384–1400.

Leopold, L. B. (1949), The interaction of trade wind and sea breeze, Hawaii, *J. Meteorol.*, *6*, 312–320.

Lu, M.-L., J. Wang, A. Freedman, H. H. Jonsson, R. C. Flagan, P. A. McClatchey, and J. H. Seinfeld (2003), Humidity halos around trade wind cumulus clouds, *J. Atmos. Sci.*, *60*, 1041–1059.

Mendonca, B. G. (1969), Local wind circulation on the slopes of Mauna Loa, *J. Appl. Meteorol.*, *8*, 533–541.

Mendonca, B. G., and W. T. Iwaoka (1969), The trade wind inversion at the slopes of Mauna Loa, Hawaii, *J. Appl. Meteorol.*, *8*, 213–219.

Nassar, R., P. F. Bernath, C. D. Boone, A. Gettelman, S. D. McLeod, and C. P. Rinsland (2007), Variability in HDO/H_2O abundance ratios in the tropical tropopause layer, *J. Geophys. Res.*, *112*, D21305 doi:10.1029/2007JD008417.

Nelson, E., R. Stull, and E. Eloranta (1989), A prognostic relationship for entrainment zone thickness, *J. Appl. Meteorol.*, *28*, 885–903.

Noone, D. (2012), Pairing measurements of the water vapor isotope ratio with humidity to deduce atmospheric moistening and dehydration in the tropical midtroposphere, *J. Clim.*, *25*, 4476–4494.

Noone, D., et al. (2011), Properties of air mass mixing and humidity in the subtropics from measurements of the D/H isotope ratio of water vapor at the Mauna Loa Observatory, *J. Geophys. Res.*, *116*, doi:10.1029/2011JD015773.

Noone, D., et al. (2013), Determining water sources in the boundary layer from tall tower profiles of water vapor and surface water isotope ratios after a snowstorm in Colorado, *Atmos. Chem. Phys.*, *13*, 1607–1623.

Price, S., and J. C. Pales (1963), Mauna Loa Observatory: The first five years, *Mon. Weather Rev.*, *91*, 665–680.

Sayres, D. S., et al. (2010), Influence of convection on the water isotopic composition of the tropical tropopause layer and tropical stratosphere, *J. Geophys. Res.*, *115*, D00J20, doi:10.1029/2009JD013100.

Schmidt, M., K. Maseyk, C. Lett, P. Biron, P. Richard, T. Bariac, and U. Seibt (2010), Concentration effects on laser-based $\delta^{18}O$ and $\delta^{2}H$ measurements and implications for the calibration of vapour measurements with liquid standards, *Rapid Commun. Mass Spectrom.*, *24*, 3,553–3,561.

Sharp, Z. (2007), *Principles of Stable Isotope Geochemistry*, 344 pp., Pearson Prentice Hall, Upper Saddle River, NJ.

Stevens, B. (2002), Entrainment in stratocumulus topped mixed layers, *Q. J. R. Meteorol. Soc.*, *128*, 2663–2690.

Sullivan, P. P., C.-H. Moeng, B. Stevens, D. H. Lenschow, and S. D. Mayor (1998), Structure of the entrainment zone capping the convective atmospheric boundary layer, *J. Atmos. Sci.*, *55*, 3042–3064.

Träumner, K., C. Kottmeier, U. Corsmeier, and A. Wieser (2011), Convective boundary-layer entrainment: Short review and progress using Doppler lidar, *Boundary-Layer Meteorol.*, *141*, 369–391, doi:10.1007/s10546-011-9657-6.

Tremoy, G., F. Vimeux, O. Cattani, S. Mayaki, I. Souley, and G. Favreau (2011), Measurements of water vapor isotope ratios with wavelength-scanned cavity ring-down spectroscopy technology: New insights and important caveats for deuterium excess measurements in tropical areas in comparison with isotope-ratio mass spectrometry, *Rapid Commun. Mass Spectrom.*, *25*, 3469–3480.

Worden, J., D. Noone, K. Bowman, and T. E. S. Team Members (2007), Importance of rain evaporation and continental convection in the tropical water cycle, *Nature*, *445*, 528–532.

Yang, Y., Y.-L. Chen, and F. M. Fujioka (2008), Effects of trade-wind strength and direction on the leeside circulation of the island of Hawaii, *Mon. Weather Rev.*, *136*, 4799–4818.

Yokelson, R., et al. (2007), Emissions from forest fires near Mexico City, *Atmos. Chem. Phys.*, *7*, 5569–5584.